Research Article | Vol. 29, No. 25 / 6 Dec 2021 / Optics Express 41447

Optics EXPRESS

Concentric tubes silicon-based metamaterial structure for mid-IR broadband absorption

MAHMOUD A. A. ABOUELATTA,[1] MUHAMMAD A. OTHMAN,[1] MAI DESOUKY,[1] AHMED M. MAHMOUD,[1,2] AND MOHAMED A. SWILLAM[1,*]

[1]*Nanophotonics Research Laboratory, Department of Physics, The American University in Cairo, Cairo 11835, Egypt*
[2]*School of Engineering and Applied Sciences, Nile University, Giza, Egypt*
[*]*m.swillam@aucegypt.edu*

Abstract: In this work, we are proposing a silicon (Si) based concentric tube broadband absorber. The proposed broadband absorber is composed of consecutive concentric tubes of intrinsic Si and doped-Si (D-Si) layers. The structure exhibits a broadband performance within a wide range of mid-IR wavelength spectrum extending from 3 to 7 μm with an absorption peak that varies between 0.88 and 0.97 in the case of S-polarized incident light. We report that light coupling to the proposed concentric tube metamaterial absorber structure over a broad wavelength range is a result of exhibiting multiple resonance mechanisms at different wavelengths. We further show that bulk plasmon polaritons are excited within the layers leading to this noticeable absorption. We demonstrate CMOS compatible metamaterial absorber that is less dependent on polarization and angle. Furthermore, this proposed design reveals new avenues to realize silicon-based broadband absorption for mid-IR photo detection and mid-IR thermal harvesting applications.

1. Introduction

Broadband absorbers are essential components for energy harvesting applications, e.g., thermal photovoltaics [1], stealth technology [2] and photo detectors [3]. Among the aforementioned applications, mid-IR photo detection within the wavelength regime of 3 to 5 μm is of particular interest due to the low atmospheric absorption demonstrated within this wavelength range [4]. Meanwhile, most of the investigated materials for mid-IR photo detectors are based on mercury–cadmium–telluride (MCT) which is toxic by nature, and consequently poses serious constraints for practical applications. Recently, III-V class semiconductor nano-wires have been widely adopted for mid IR photo detection. However, III-V semiconductors are expensive materials, and are not feasible for mass production [4]. Consequently, scientists are prompted to explore cost competitive mid-IR absorbing materials that are CMOS compatible, and can be fabricated by standard lithography techniques. Metamaterials (MMs) have drawn significant attention in the research community due to their diverse applications and implementations in different engineering aspects. These applications include: sub-wavelength focusing [5,6], spontaneous emission manipulation [7,8] and cloaking [9]. MMs have been reported to realize unity absorption via impedance matching between incident radiation and the designed MMs, however, tuning the magnetic permeability -to achieve perfect impedance matching- is not a trivial task to be implemented [10,11]. Studies which have precluded the application of grating, proposed tapered structures which show very high broadband absorption values [12–15]. Nevertheless, designs as such, include expensive metals which might not be useful for mid IR photo detection. Furthermore, planar structures often experience delamination and lattice mismatch constraints when different constituent materials are used. In order to overcome the aforementioned obstacles, single material-based structures represent a good solution for mid IR absorption [3]. We previously demonstrated that Si/D-Si layered metamaterial absorber

#441105 https://doi.org/10.1364/OE.441105
Journal © 2021 Received 20 Aug 2021; revised 27 Oct 2021; accepted 28 Oct 2021; published 30 Nov 2021
Corrected: 1 December 2021

Optics EXPRESS

integrated with specifically designed multiple diameter or multiple height gratings can lead to mid-IR broadband absorption, reaching absorption values as high as 0.97 [3].

In this work, we study the absorption in the mid-IR wavelength range using Si/D-Si concentric tubes absorber without the need to design complex grating structure. Different parameters have been tested like filling ratios, periods, and angle of incidence. We propose intrinsic Si/D-Si tubes that can achieve a broadband absorption of more than 0.9 for a certain band in the mid-IR range from 3 to 7 μm. We found that our proposed structure is angle less-dependent and polarization less-dependent for a wide range in the band of the study. In addition, the simplicity of concentric cylindrical structures will make designing it a straightforward task compared to their planar counterparts. This proposed design is fully Si based and can be fabricated by conventional Si fabrication methodologies.

2. Theoretical study

The structure is comprised from 10 concentric cylinders of N-doped Si (D-Si) acting as the metallic layer and intrinsic Si acting as the dielectric layer, as shown schematically in Fig. 1(a). The layer thickness is given by t and the tube length L is chosen to be 4 μm. An air core is introduced in the tubes defined as d_c and the period of unit cell is given by p. We used the Finite difference time domain (FDTD) method for simulating a transverse electric (TE) polarized plane wave normally incident from the bottom of the structure. A single cell of the structure has been simulated where Bloch boundary conditions were applied in the x and y directions to take into account the periodic structure whereas a perfectly matched layer was applied in the z-direction as can be seen in Fig. 1(b). Two monitors were placed in the FDTD region, where one is in front of the source beyond the Si/D-Si concentric tubes metamaterial absorber to measure transmission (T), and the other monitor is behind the source to measure the reflection (R). Thus, absorption (A) can be measured as follows: $A = 1 - (R + T)$.

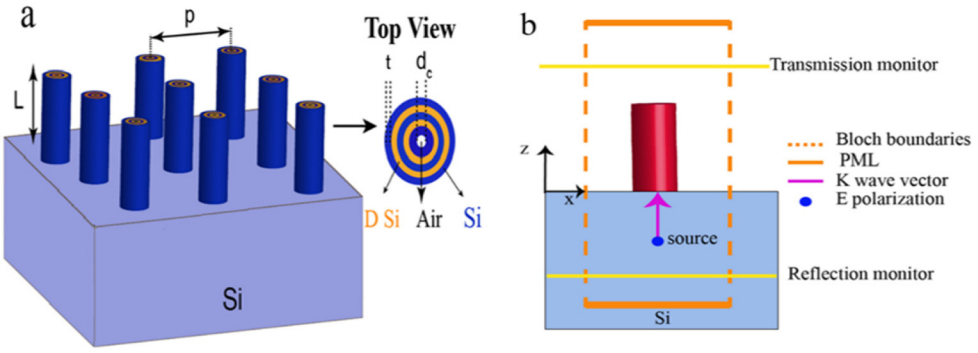

Fig. 1. Schematic for periodic Si/D-Si concentric tubes absorber. a) An air core with diameter (d_c) 200 nm is introduced in the concentric tubes. The period is given by p and layer thickness is given by t. b) schematic used in Lumerical FDTD for simulating the proposed structure.

Drude's model has been used to study the dispersion of doped-Si as follows [16]:

$$\varepsilon_m(\omega) = \varepsilon_\infty - \frac{{\omega^2}_p}{\omega^2 + i\omega\gamma} \tag{1}$$

$$\omega_p = \sqrt{\frac{N_d\, q^2}{\varepsilon_0\, m^*}} \tag{2}$$

Optics EXPRESS

where ε_m is the complex permittivity of doped-Si (shown in Fig. 2), γ is the damping term (collision frequency) of value $\frac{q}{\mu m^*} = 17.1 \times 10^{13}$rad/s, ε_∞ is the static permittivity of value 11.7, ω_p is the plasma frequency (2.2×10^{15} rad/s) at certain doping concentration N_d and m* is the effective mass of value 0.26 m (where m is the electron rest mass).

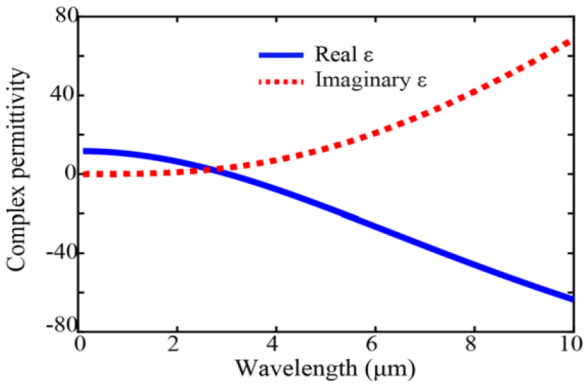

Fig. 2. Complex permittivity of doped Si (D-Si) of N_d of 4×10^{20} cm^{-3}.

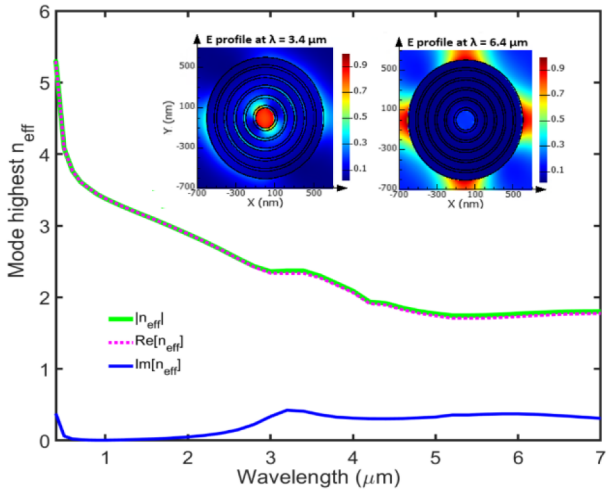

Fig. 3. The effective index of the fundamental mode supported by the structure (the highest effective index) at different wavelengths for a cross section of proposed structure with a filling ratio of 3:1 Si:D-Si. The inset shows the electric field profile **E** of the fundamental mode at $\lambda = 3.4$ μ (bulk plasmon polariton [18]) and $\lambda = 6.4$ μ (long-range plasmon [18]), where the confinement of the electric field to the concentric tubes, decreases by increasing the wavelength.

To understand the behavior of the concentric tubes' absorber, we conducted another simulation to get the effective refractive index of the concentric tubes structure at different wavelengths. The objective here is to study quantitively how the structure in its configuration may get a lower effective index compared to silicon which is 3.5 as well as the doped silicon refractive index, shown in Fig. 2. Theoretically, a good absorber is a structure that has a minimum reflection once a wave is incident on it. In this simulation, the incident wave is assumed to be propagating from air as medium 1 hitting the absorber which is medium 2. Whenever medium 2 effective refractive

Optics EXPRESS

index becomes closer to the value of refractive index of the medium 1 (which has a value of 1 here for air), then a good absorber can be achieved due to the fact that A = 1 − (R + T). This can be considered valid as long as the effective index of the structure decreases below the value of Si and D-Si. By inspecting Fig. 3, it is evident that the absolute effective refractive index of the structure decreased to about 1.7 starting from the band of 4 μm.

The modal analysis of the structure sheds some light on the behavior of the electric field and how the absorption takes place. The doped silicon material in the eigen mode calculations is modelled by the Drude's model. In Fig. 3. it is shown that for larger wavelengths, the electric field starts to scatter outside the concentric tubes, and starts to localize between each set of the concentric tubes. For shorter wavelengths, the main absorbed power happens through the concentric tubes itself in addition to the air gap in the middle of the structure. The inset of Fig. 3. shows the electric field profile E inside the concentric tubes at λ = 3.4 μ and λ = 6.4 μ where for the later wavelength, no electric field is coupled inside the concentric tubes. So, we have 2 different locations for absorbing the incident power depending on the wavelength and that stands behind the broad spectrum of the absorber.

3. Results and discussion

We proceed to study the broadband absorption (BBA) in our designed concentric tubes metamaterial absorber. Figure 4(a) shows the BBA for Si/D-Si concentric tubes metamaterial absorber designed with a filling ratio of 3:1 for Si to D-Si, respectively, with a total thickness of 0.5 μm (The total number of layers is 10, 5 Si layers and 5 doped-Si layers, the thickness of the Si layer is 75 nm and the thickness of the doped-Si is 25 nm), L = 4 μm, d_c = 200 nm, and p = 1.4 μm. Figure 4(a) shows a broad absorption band within the wavelength range from 3 μm to 7 μm with an absorption varying between 0.88 to 0.77 for a transverse electric (TE) polarized light normally incident on the concentric tubes metamaterial absorber.

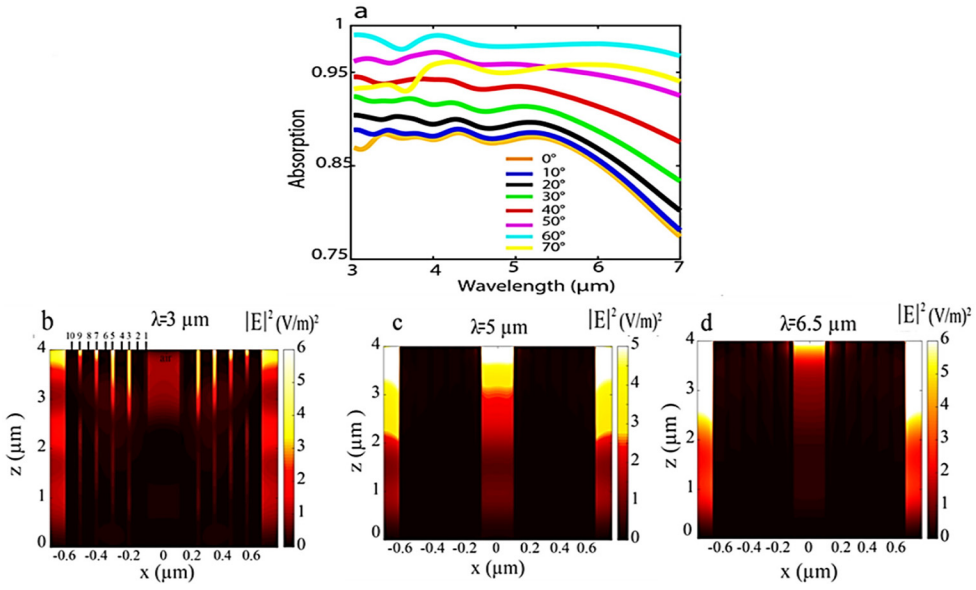

Fig. 4. FDTD absorption results. a) Absorption of Si/D-Si tubes at normal and oblique incidence from 0 to 70 degrees at TE incidence, b-d) show the electric field distribution $|E|^2$ for Si/D-Si tubes at different wavelengths, which are b) 3 μm, c) 5μm, and d) 6.5 μm.

Optics EXPRESS

The maximum and minimum absorption values were selected through the previously specified wavelength range and similarly for the rest of this work. Also, for the same figure (Fig. 4(a)), it is obvious that increasing the angle of incidence from 0° to 60° slightly increases the BBA values, where the maximum absorption can be realized at angle 60° with absorption value reaching a value of 0.97. Thus, the proposed tubes demonstrate an angle less-dependent broad absorption band at the mid IR wavelength range. Furthermore, having a periodic structure of D-Si can enhance the absorption to more than 0.6 for wavelength range varying between 3 to 7 μm due to the multiple loss mechanisms introduced by the charge carriers of D-Si. However, having Si/D-Si tubes lead to enhancing the absorption to a value of more than 0.8 at normal incidence and near 0.97 at oblique incidence which remains nearly high for the entire studied wavelength range of 3 to 7 μm.

Generally, these concentric tubes can support increased number of propagating light modes due to the large density of available photonic states associated with the iso-frequency surface [17]. Enhancing coupling between the incidence light and the modes results in realizing multiple loss mechanisms at different wavelengths leading to broadband absorption. Furthermore, the presence of a periodic array with an air core in the tubes forms a photonic crystal that provides another form of resonance mechanism depending on the dimension of the air core diameter. In order to illustrate the excitation of multiple loss mechanisms, Figs. 4(b-d). show the electric field intensity $|E|^2$ profile at discrete wavelengths across the investigated wavelength of interest. This can be attributed to bulk plasmon modes that are highly confined to the bulk of the layered material [18]. We deduced using the modal field distributions for the short wavelengths (such as 3000, and 3400 nm) that these modes are bulk plasmon modes since they are highly confined to the bulk of the layered material in our work [18]. Moreover, the coupling of surface plasmon polaritons (SPPs) leads to the formation of long-range plasmon modes [18]. Hence, it can be concluded that the supported modes for the longer wavelengths (such as 6400 nm) originate from the surface plasmon polaritons since they have a field distribution similar to the field distribution of the long-range plasmons (high intensity outside the bulk of layered material and low-intensity inside it [18]). Figure 4(b). reveals high field confinement inside the concentric tubes metamaterial absorber layers among the Si/D-Si interface at wavelength of 3 μm. Moreover, this behavior holds on up to a wavelength of 4 μm. This can be attributed to the fact of excitation of bulk plasmon polaritons in concentric tubes metamaterial absorber layers, where those collective plasmon oscillations provide multiple photonic states to couple with the incident light. Here, we attribute the absorption within the regime from 3 to 4 μm due to the presence of multiple tubes of different diameters, where each tube with a specific diameter can match the momentum of incident light at a particular wavelength range, hence, resulting in a broad absorption across the wavelength range of interest. Figure 4(b) reveals a high electric field intensity in the air core at a wavelength of 5 μm, this field profile holds on to a wavelength range of nearly 6.2 μm. The air core introduced in such a design is surrounded by a D-Si interface, which results in a surface plasmon wave propagating at the air/D-Si interface. Thus, introducing an air core in the tubes excites another form of pronounced resonance that facilitates coupling to the incident light at a certain wavelength range. Moving further to a longer wavelength range, Fig. 4(d) indicates vanishing of the electric field intensity from inside the concentric tubes metamaterial absorber and the air core, whereas it becomes more pronounced at the external interface between each whole concentric tubes metamaterial absorber with one another. This behavior is only recognized at the longer wavelength range beyond 6.2 μm.

Therefore, coupling of incident light to concentric tubes metamaterial absorber can be realized when a strong resonance mechanism is supported on a broad spectrum of wavelengths. Absorption of tubes can be tailored based on several parameters; first, a proper design of sub-wavelength doped semiconductor/semiconductor interface that can support bulk plasmons among its momentum space. Secondly, tailoring the air core diameter of the photonic crystal to be sub-wavelength as

Optics EXPRESS

well. Thirdly, a proper choice of the external tube-to-tube distance that guarantees near field interaction between them.

We proceed with further analysis to investigate the effect of different design parameters on the performance of the concentric tubes metamaterial absorber. The tubes are designed with four different variable parameters which are; layer thickness t, period p, air core diameter d_c and tube length L as indicated in Fig. 1. The tubes length is taken to be constant across the whole study, since it is assumed to be less effective in altering the absorption behavior of the Si/D-Si concentric tubes metamaterial absorber. Figure 5(a) shows the effect of varying the layer thickness indicated in terms of the ratio of Si to D-Si as follows; 1:3 (25 nm Si to 75 nm D-Si), 1:1 (50 nm Si to 50 nm D-Si), 3:1 (75 nm Si to 25 nm D-Si), and 9:1 (90 nm Si to 10 nm D-Si). It can be clearly seen that, as the thicknesses of intrinsic Si increases with respect to D-Si from ratio of 1:3 (Si: D-Si) to ratio of 3:1 (Si: D-Si), the absorption increases which is due to the reduction in losses introduced by the charge carriers in D-Si. This can be explained, based on the fact that the supported modes would not couple efficiently to the incident wave, and most of the energy would be reflected due to the impedance mismatch. In other words, increasing the density of lossy materials in the structure is a trade-off. From one side, it increases the loss coefficients of the structure modes. However, it makes the coupling efficiency of the incident wave with the supported modes of the structure much lower. Moreover, as we illustrated in Fig. 3, the absorption reaches a maximum when the supported modes of the structure are more likely to couple with the incident wave. Consequently, when the thickness of Si is increased to 90 nm with respect to 10 nm of D-Si, the absorption drops significantly due to degradation of the behavior as a result of having very high filling ratio of dielectric. As previously mentioned, the concentric tubes metamaterial absorber performance relies on metal/ dielectric filling ratio to shape the dispersion momentum space. Decreasing the doped semiconductor component filling ratio decreases the magnitude of the real negative part of the effective permittivity in which the whole composite system can act more as a dielectric rather than as a metamaterial, thus, the absorption will be consequently lowered.

Figure 5(b) shows the effect of varying the air core diameter on the absorption of Si/D-Si concentric tubes metamaterial absorber. It can be clearly seen that having an air core inside the concentric tubes metamaterial absorber alters the absorption at the longer wavelength range. For concentric tubes metamaterial absorber of zero air core diameter, there is a significant drop in the absorption band beyond 4.7 μm, however, introducing an air core raises the absorption to more than 20% at 5.5 μm. It is also demonstrated within the same figure that; the absorption slightly varies for different air core diameters. For air core of diameter 200 nm and 300 nm, the absorption is near 0.8 at λ of 7 μm as compared to nearly 0.73 for a 100 nm air core diameter.

This can be explained as follows; introducing an air core acts as a dielectric medium surrounded by the metallic interface of D-Si. Such an air/D-Si periodically structure is quite similar in behavior with a photonic crystal [17], which can resonate with the incoming light at a particular wavelength depending on the dimension of the air core diameter. Furthermore, the air core diameter is surrounded by the D-Si interface, which will result in a surface plasmon wave propagating at the air/D-Si interface. Moreover, the air core diameter is surrounded by a D-Si interface, which results in surface plasmon wave propagating at the air/D-Si interface, thus introducing an air core leads to another form of pronounced resonance in the proposed design as previously mentioned. It is still not clear the reason that some air core diameters show higher absorption as compared to another, and that should be addressed in detail in future work.

However, the effect of the air core diameter is obvious in enhancing the absorption at the longer wavelength range. We used an air core of diameter 200 nm throughout our study where it reveals the highest absorption at the longer wavelength range for this proposed design. Figure 5(c) shows the effect of the variation of period on the absorption mechanism. It is obvious that the period value has a minor effect on tuning the absorption mechanism. For a period of 1.2 μm where

Optics EXPRESS

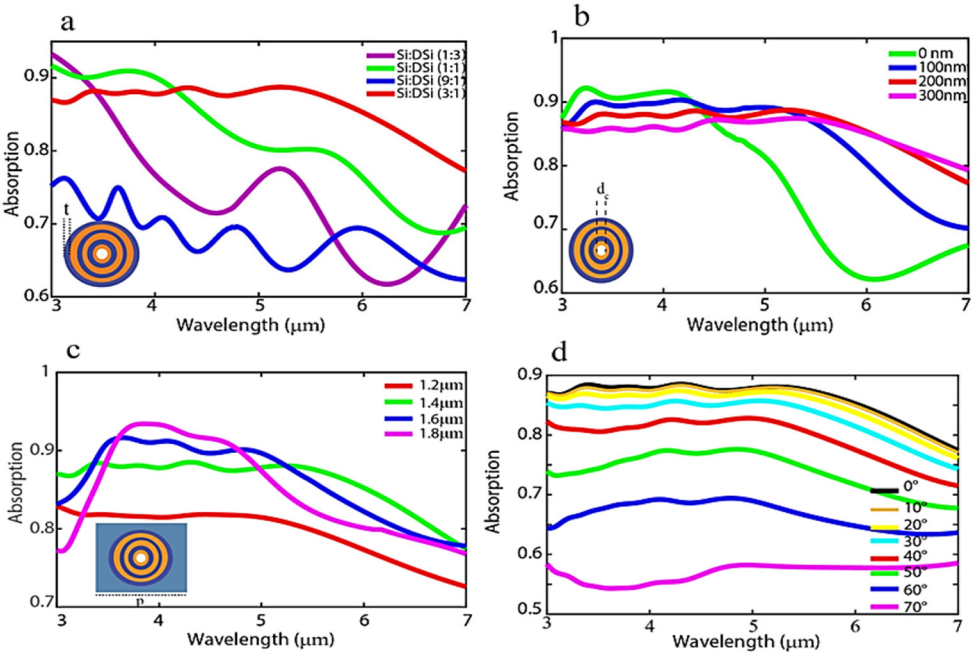

Fig. 5. Absorption of Si/D-Si hyperbolic tubes: a) at different thicknesses of Si: D-Si layers which are; (25:75 nm), (50:50 nm), (75:25 nm) and (90:10 nm), b), at different thicknesses of the air core diameter which are; 0, 100, 200 and 300 nm, c) at different periods; 1.2, 1.4, 1.6 and 1.8 μm and d), Absorption of Si/D-Si hyperbolic tubes at normal and oblique incidence from 0 to 70 degrees at a TM incidence.

the concentric tubes of the metamaterial absorber adhere to each other, the least absorption is addressed as compared to non-touching tubes. As previously indicated in Fig. 4(d), there is a resonance mechanism taking place between each unit cell with one another, thus, for closely packed/touching tubes, this kind of resonance could vanish, and as a consequence, the absorption could be lowered as compared to non-touching absorber tubes. Therefore, the effect of varying the distance between the tubes is less pronounced in tuning the absorption mechanism.

In order to confirm that our absorber is polarization less-dependent, which is an important feature for efficient absorbers, we tested this attribute by illuminating our concentric tubes metamaterial absorber with a transverse magnetic (TM) polarized light. Figure 5(d), shows the absorption for the concentric tubes metamaterial absorber tubes in case of TM incidence, which reveals high absorption values comparable to the absorption resulted from the TE polarized light at normal incidence (previously indicated in Fig. 4(a)). However, in Fig. 5(d), the absorption remains high up till an angle of 50°, further increase in angle of incidence reduces the absorption dramatically as can be seen in case of angle 70°. Thus, indicating that this proposed absorber is polarization less-dependent, but slightly angle dependent in case of TM incidence. It is worth noting that due to the symmetry of the structure in the XY plane, the results are the same for both of the TE and TM components at normal incidence. This symmetry matches the reported results for the angle of (0°) incidence in Fig. 4(a) and Fig. 5(d). However, for oblique incidence, the electric field would only have an X-component (transverse component) for the TE incidence, while it would have both a Y-component (horizontal component) and a Z-component (vertical component) for the TM case. Consequently, the coupling of the incident wave with the supported modes of the structure would be different for both cases. Accordingly, the symmetry in the XY plane is only relevant to the normal incidence scenario. Moreover, we believe that different

Optics EXPRESS

dimensions of the tubes account for extending and boarding of the absorption spectrum in a close behavior to the elliptical fractal metamaterial absorber [19], but in a circular manner rather than elliptical.

4. Structure fabrication

Periodic Si tubes can be fabricated by standard photolithography, and then deep reactive ion etching (DRIE) is applied on a commercial Si wafer. Then, plasma enhanced chemical vapor deposition (PECVD) can be applied to deposit the subsequent D-Si/Si layers where N-doping of Si can be performed during the PECVD process. By controlling the process parameters,

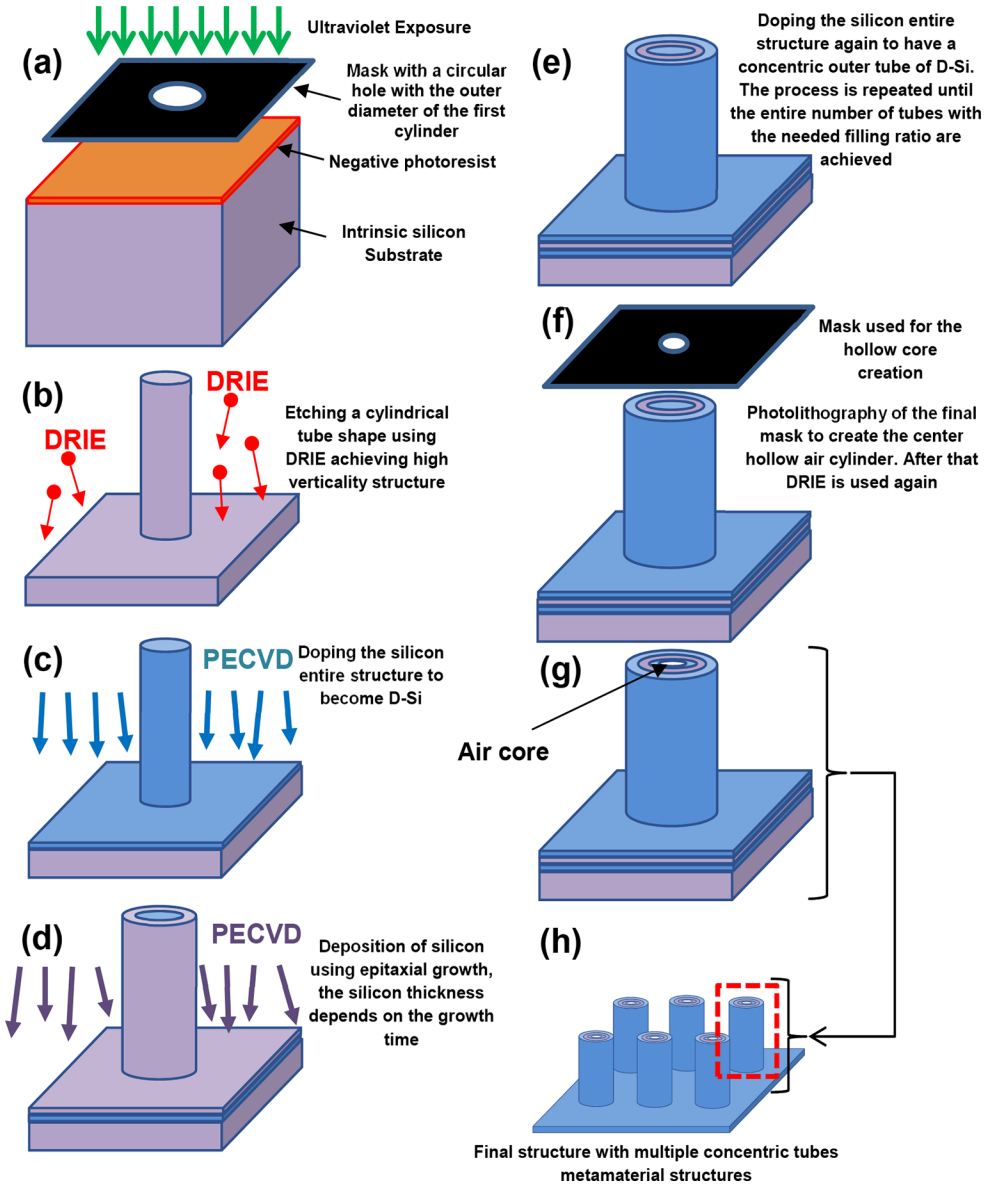

Fig. 6. Concentric tubes silicon-based metamaterial structure fabrication steps.

Optics EXPRESS

temperature, and deposition time, perfect control over each layer thickness is manageable, thus, a periodic pattern of alternating Si/D-Si layers is obtained. We show the fabrication steps for a single rod composed of multiple concentric rings and the structure can be repeated in the lateral 2 directions using the adequate mask. The mask can be a circular perforated pattern of chrome over quartz glass substrate where the circular pattern on the mask has the outer diameter of the central rod, as shown in Fig. 6(a), using a negative photoresist. Moreover, another technique can be used for creating high aspect ratio nanostructures [20] where the realized structure has a relatively square shape rather than circular one. This square shape structure can be relatively rounded using isotropic etching of Si. After the whole planer structure with multiple rods is fabricated, as shown in Fig. 6(b), using DRIE, doping of the first layer of D-Si is created, as shown in Fig. 6(c). Then, a subsequent deposition of a Si layer is achieved using PECVD, as shown in Fig. 6(d). The process is repeated until the required number of the concentric tubes is achieved. Finally, the air core is created using a similar mask as the starting one, but with a circular hole with the dimensions of the central air core, as shown in Fig. 6(f)-(g). Finally, the entire fabricated structure is shown in Fig. 6(h).

5. Conclusion

In this work, we have demonstrated a broadband mid-IR absorber using Si/D-Si tubes with an absorption reaching a peak of nearly 0.88-0.97 from 3 to 7 μm in case of the TE incident light. We have shown the possibility of designing a polarization less-dependent and angle less-dependent absorber within some limitations. We have proposed an all Si, cost effective absorber which can be fabricated by standard Si fabrication techniques in contrary to many other metamaterial absorbers that rely on phase change materials which are not CMOS compatible. We provide a protocol for this proposed design to show its ease in fabrication using conventional lithography techniques. Finally, this structure unravels exciting avenues to realize applications in the mid-IR range including thermal harvesters and mid-IR photodetectors. It is worth noting that this structure can serve in other wavelength ranges across the infrared regime depending on the doping concentration, thus revealing an extra advantage for using D-Si instead of metal, which is the capability to tune the absorption band across the infrared wavelength range.

Funding. Academy of Scientific Research and Technology, Egypt.

Acknowledgments. The authors acknowledge the funding from the knowledge alliance in solar energy provided through the Egyptian Academy of Scientific Research and Technology 2018 to the American University in Cairo.

Disclosures. The authors declare no conflicts of interest.

Data availability. The data that support the findings of this study are available from the corresponding author upon reasonable request.

References

1. C. Wu, B. Neuner III, J. John, A. Milder, B. Zollars, S. Savoy, and G. Shvets, "Metamaterial-based integrated plasmonic absorber / emitter for solar thermo-photovoltaic systems," J. Opt. **14**(2), 024005 (2012).
2. K. Iwaszczuk, A. C. Strikwerda, K. Fan, X. Zhang, R. D. Averitt, and P. U. Jepsen, "Flexible metamaterial absorbers for stealth applications at terahertz frequencies," Opt. Express **20**(1), 635–643 (2012).
3. M. Desouky, A. M. Mahmoud, and M. A. Swillam, "Silicon based mid-IR super absorber using metamaterial," Sci. Rep. **8**(1), 2036 (2018).
4. M. Royo, M. De Luca, and R. A. Rurali, "Review of III – V nanowire infrared photodetectors and sensors," J. Phys. D: Appl. Phys. **50**(14), 143001 (2017).
5. M. Desouky, A. M. Mahmoud, and M. A. Swillam, "Tunable Mid IR focusing in InAs based semiconductor Metamaterial," Sci. Rep. **7**(15312), 1–7 (2017).
6. A. Fang, T. Koschny, and C. M. Soukoulis, "Optical anisotropic metamaterials: Negative refraction and focusing," Phys. Rev. B **79**(24), 245127 (2009).
7. D. Lu, J. J. Kan, E. E. Fullerton, and Z. Liu, "Enhancing spontaneous emission rates of molecules using nanopatterned multilayer metamaterials," Nat. Nanotechnol. **9**(1), 48–53 (2014).
8. S.-A. Biehs, M. Tschikin, R. Messina, and P. Ben-Abdallah, "Super-Planckian near-Field thermal emission with Phonon-Polaritonic metamaterials," Appl. Phys. Lett. **102**(13), 131106 (2013).

Optics EXPRESS

9. M. Farhat, P. Y. Chen, H. Bagci, C. Amra, S. Guenneau, and A. Alu, "Thermal invisibility based on scattering cancellation and mantle cloaking," Sci. Rep. **5**(1), 9876 (2015).
10. P. Singh, K. A. Ameri, L. Chao, N. M. Afsar, and S. Sonkusale, "Broadband Millimeter wave metamaterial absorber based on embedding of dual resonators," Prog. Electromagn. Res. **142**, 625–638 (2013).
11. A. Dubey and T. C. Shami, "Metamaterials in Electromagnetic Wave Absorbers," Def. Sci. J. **62**(4), 261–268 (2012).
12. J. Zhou, A. F. Kaplan, L. Chen, and L. J. Guo, "Experiment and Theory of the Broadband Absorption by a Tapered Metamaterial Array," ACS Photonics **1**(7), 618–624 (2014).
13. Z. Jiao, R. Ning, Y. Xu, and J. Bao, "Tunable angle absorption of metamaterials based on plasma photonic crystals," Physics of Plasmas **23**(6), 063301 (2016).
14. K. V. Sreekanth, A. De Luca, and G. Strangi, "Excitation of volume plasmon polaritons in metal-dielectric metamaterials using 1D and 2D diffraction gratings," J. Opt. **16**(10), 105103 (2014).
15. S. He, F. Ding, L. Mo, and F. Bao, "Light Absorber with an Ultra-Broad Flat Band Based on Multi-Sized Slow-Wave Metamaterial Thin-Films," Prog. Electromagn. Res. **147**, 69–79 (2014).
16. R. Gamal, Y. Ismail, and M. A. Swillam, "Silicon Waveguides at the Mid-Infrared," J. Lightwave Technol. **33**(15), 3207–3214 (2015).
17. C. T. Riley, J. S. T. Smalley, J. R. J. Brodie, Y. Fainman, and D. J. Sirbuly, "Near-perfect broadband absorption from metamaterial nanoparticles," Proc Natl Acad Sci USA **114**, 6 (2016).
18. I. Avrutsky, I. Salakhutdinov, J. Elser, and V. Podolskiy, "Highly confined optical modes in nanoscale metal-dielectric multilayers," Phys. Rev. B **75**(24), 241402 (2007).
19. R. M. H. Bilal, M. A. Saeed, P. K. Choudhury, M. A. Baqir, W. Kamal, M. M. Ali, and A. A. Rahim, "Elliptical metallic rings-shaped fractal metamaterial absorber in the visible regime," Sci. Rep. **10**(1), 14035 (2020).
20. Z. Ma, T. Guo, S. Cheng, Z. Song, J. Wang, and W. Yuan, "Fabrication of ultrahigh-aspect-ratio and periodic silicon nanopillar arrays using dislocation lithography and deep reactive-ion etching," J. Micromech. Microeng. **29**(10), 105011 (2019).